nature medicine

A small molecule blocking oncogenic protein EWS-FLI1 interaction with RNA helicase A inhibits growth of Ewing's sarcoma

Hayriye V Erkizan[1], Yali Kong[1], Melinda Merchant[2], Silke Schlottmann[1], Julie S Barber-Rotenberg[1], Linshan Yuan[1], Ogan D Abaan[1], Tsu-hang Chou[2], Sivanesan Dakshanamurthy[1], Milton L Brown[1], Aykut Üren[1] & Jeffrey A Toretsky[1,3,4]

Many sarcomas and leukemias carry nonrandom chromosomal translocations encoding tumor-specific mutant fusion transcription factors that are essential to their molecular pathogenesis. Ewing's sarcoma family tumors (ESFTs) contain a characteristic t(11;22) translocation leading to expression of the oncogenic fusion protein EWS-FLI1. EWS-FLI1 is a disordered protein that precludes standard structure-based small-molecule inhibitor design. EWS-FLI1 binding to RNA helicase A (RHA) is important for its oncogenic function. We therefore used surface plasmon resonance screening to identify compounds that bind EWS-FLI1 and might block its interaction with RHA. YK-4-279, a derivative of the lead compound from the screen, blocks RHA binding to EWS-FLI1, induces apoptosis in ESFT cells and reduces the growth of ESFT orthotopic xenografts. These findings provide proof of principle that inhibiting the interaction of mutant cancer-specific transcription factors with the normal cellular binding partners required for their oncogenic activity provides a promising strategy for the development of uniquely effective, tumor-specific anticancer agents.

There is a considerable need for new cancer therapies that enhance efficacy and reduce long-term morbidity. Protein products of tumor-specific chromosomal translocations provide unique targets for anti-tumor therapies[1]. These translocations span a broad range of malignancies, including carcinomas, hematopoietic malignancies and sarcomas[2–4]. In many cancers, these translocations lead to new fusion proteins that both initiate and maintain oncogenesis. Although some of these translocations, such as breakpoint cluster region–Abelson oncoprotein (BCR-ABL)[5], lead to constitutively activated kinases, the majority lead to fusion proteins that function as transcription factors and lack intrinsic enzymatic activity. These translocation-generated transcription factor fusion proteins are ideal targets of anticancer therapies, yet no specific pharmaceuticals have been developed to date.

The ESFTs are undifferentiated tumors that can occur anywhere in the body, most often in the second and third decades of life. ESFTs often respond well to initial chemotherapy, yet 40% of patients will develop lethal recurrent disease. Seventy-five to eighty percent of people who present with metastatic ESFTs will die within 5 years, despite high-dose chemotherapy[6]. ESFTs contain a well-characterized chromosomal translocation that fuses the amino half of EWS to the carboxy half of an *ets* (erythroblastosis virus E26 transforming sequence gene) family DNA binding protein[7]. The most common fusion protein is the oncogenic transcription factor EWS-FLI1. Elimination of EWS-FLI1 through antisense and small interfering RNA approaches results in the prolonged survival of ESFT xenograft–bearing mice[8], but this approach currently lacks translation to clinical therapy[9,10]. As EWS-FLI1 lacks intrinsic enzymatic activity, small-molecule targeting would be directed toward the disruption of EWS-FLI1 from established transcriptional complexes. The EWS-FLI1 transcriptional complex includes: RNA polymerase II, cyclic AMP response element–binding protein and RHA[11–13]. Our previous investigations showed that RHA augments EWS-FLI1–modulated oncogenesis, suggesting that this protein-protein complex is particularly essential for tumor maintenance[13]. Small-molecule inhibitors that block RHA interaction by targeting the oncogenic fusion protein EWS-FLI1 would be the first in a new class of antitumor therapy directed at these proteins.

RHA has a crucial role in embryogenesis and thus might be a reasonable option as a partner for an oncoprotein in undifferentiated tumors and is indispensable for ectoderm survival in gastrulation of mammals[14]. RHA is also required beyond embryogenesis because RHA-null mouse fibroblast cells are not viable (C.-G. Lee (University of Medicine and Dentistry of New Jersey), personal communication). However, transient reduction of RHA protein expression in COS cells did not affect their viability[15]. RHA provides a transcriptional coactivator role in models of tumorigenesis, and in the nuclear factor-κB (NF-κB)[16] and signal transducer and activator of transcription-6 (ref. 17) transcriptomes. RHA binds DNA in a sequence specific manner within the promoters of the genes encoding cyclin-dependent kinase inhibitor 2A (ref. 18) and multidrug resistance protein-1

[1]Georgetown University, Lombardi Comprehensive Cancer Center, Department of Oncology, Washington, DC, USA. [2]Memorial Sloan-Kettering Cancer Center, New York, New York, USA. [3]Georgetown University, Department of Pediatrics, Washington, DC, USA. [4]Correspondence should be addressed to J.A.T. (jat42@georgetown.edu).

Received 2 March; accepted 8 May; published online 5 July 2009; doi:10.1038/nm.1983

(ref. 19). The amino-terminal region of RHA is most often the site for protein-protein interactions. cAMP-binding protein binds amino acids 1–250 of RHA[20], RNA polymerase II and breast cancer protein-1 (ref. 21), and RNA-induced silencing complex components[22] bind in the amino-terminal region. EWS-FLI1 binds RHA in a unique region that is not occupied by other transcriptional or RNA metabolism proteins[13], thus increasing the attractiveness of this protein-protein interaction target.

Disruption of protein-protein interactions by small molecules is a rapidly evolving field. Proteins with more flexible structures, in some cases disordered proteins, have a greater potential for small-molecule binding than rigid proteins because of higher induced-fit sampling probabilities[23]. A disordered protein is defined, in part, by increased intrinsic movement and the inability to form rigid three-dimensional structures (reviewed in ref. 24). EWS-FLI1 is a disordered protein and requires the disorder for maximal transactivation of transcription[25,26]. On the basis of these observations, EWS-FLI1, along with its binding to RHA, may provide a unique drug target even without structural information of the EWS-FLI1 protein.

RESULTS

RHA is a validated target in ESFTs

A region of RHA that binds EWS-FLI1 was identified based upon phage-display epitope screening[13] (**Fig. 1a**). To validate RHA as essential for the survival of ESFT cells, we lowered RHA levels with short hairpin RNA (shRNA), and ESFT cell viability was reduced by 90% (**Fig. 1b**,**c**). We stably transfected PANC1 cells, a pancreatic cell line that does not express EWS-FLI1, with the same shRNA vectors, yielding a similar reduction in RHA abundance (**Supplementary Fig. 1a**) but with no decrease in cell viability (**Supplementary Fig. 1b**). We further validated the RHA and EWS-FLI1 interaction with site-directed mutagenesis in the GST-RHA$_{647–1075}$ fragment to identify mutants that don't interact with EWS-FLI1. We expressed GST-RHA$_{647–1075}$ mutants and immunoprecipitated them with full length recombinant EWS-FLI1. Mutants P824A and D827A showed a significant decrease in binding to EWS-FLI1 compared to wild-type control RHA (P = 0.0129 and P= 0.0034, respectively; **Fig. 1d**). The full-length RHA mutant D827A maintained wild-type ATPase activity (**Supplementary Fig. 2**); therefore, we chose the D827A mutant to test whether RHA binding to EWS-FLI1 is required for neoplastic transformation.

We stably transfected mouse embryonic fibroblasts (W cells) that express low levels of endogenous RHA[13] with EWS-FLI1 (WEF1 cells) and either full-length wild-type RHA or full-length RHA D827A. We observed a greater than additive effect of RHA and EWS-FLI1 expression on anchorage independent growth when comparing the colony numbers from W cells expressing RHA (227 ± 66 colonies) and WEF1 cells (115 ± 8 colonies) to those of WEF1 cells expressing RHA (582 ± 30 colonies) (**Fig. 1e**,**f**). The RHA D827A–expressing cells showed a 60% reduction in anchorage-independent growth (P = 0.0028) compared to cells expressing wild-type RHA (**Fig. 1e**,**f**). We quantified EWS-FLI1 expression by densitometry of the immunoblot (**Fig. 1g**,**h**). The markedly lower colony formation by the RHA D827A–expressing cells suggests a crucial role of RHA for transforming activity of EWS-FLI1 that is abrogated by RHA not binding to EWS-FLI1.

E9R peptide disrupts binding and inhibits growth

As RHA is necessary for optimal EWS-FLI1 activity, we developed reagents to block RHA binding to EWS-FLI1. The E9R peptide corresponds to amino acids 823–832 of RHA. With the immunoprecipitation assay, we assessed binding between bacterially expressed GST-RHA$_{647–1075}$ and full-length purified recombinant EWS-FLI1 (**Fig. 2a**). Titration of E9R showed a dose-dependent reduction in the binding of GST-RHA$_{647–1075}$ and full-length EWS-FLI1 with a decreased association to 50% with 0.1 μM E9R (**Fig. 2a**). We thus sought to determine whether disrupted EWS-FLI1–RHA binding inhibits cell growth.

Peptide delivery to growing cells is greatly facilitated by cell-permeable peptides (CPP)[27]. We fused the CPP antennapedia to the amino terminus of E9R or with the D827A mutation (E9R-P and

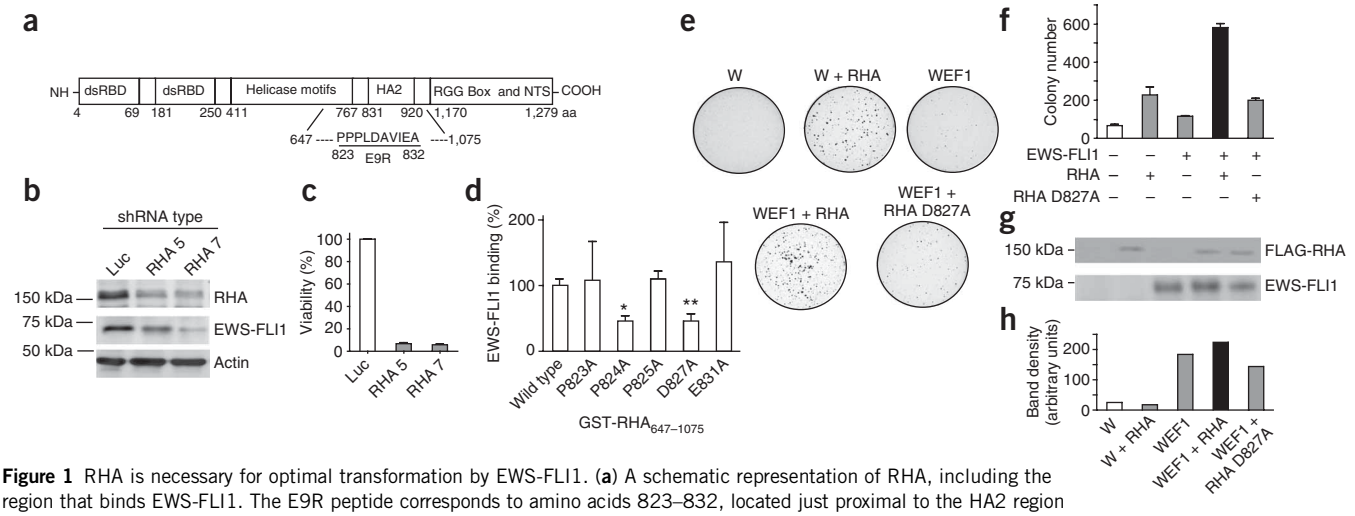

Figure 1 RHA is necessary for optimal transformation by EWS-FLI1. (**a**) A schematic representation of RHA, including the region that binds EWS-FLI1. The E9R peptide corresponds to amino acids 823–832, located just proximal to the HA2 region of RHA. dsRBD, double-stranded RNA–binding domain, RGG box, arginine glycine glycine box; NTS, nuclear transport signal; aa, amino acid residue. (**b**) An shRNA expression vector was transfected into TC71 (ESFT) cells to reduce RHA levels. (**c**) TC71 viability after RHA knockdown, as measured by cell proliferation reagent water-soluble terazolium salt (WST) reduction. (**d**) Alanine mutagenesis within E9R sequence was followed by *in vitro* immunoprecipitation with EWS-FLI1. The density of the GST-RHA band was measured, and this graph is the average of three experiments. RHA P824A and D827A mutants have significantly lower binding to EWS-FLI1 (*P = 0.0129 and **P = 0.0034, respectively). (**e**) Mouse fibroblasts were placed in soft agar for anchorage-independent growth assays (empty vector (W), EWS-FLI1 alone (WEF1)). (**f**) The graph enumerates the colonies counted in three separate experiments. (**g**) Protein expression of fibroblasts, detected with antibody to Flag (top) or antibody to FLI1 (bottom). (**h**) Densitometry of the EWS-FLI1 blot, performed with MultiGauge software.

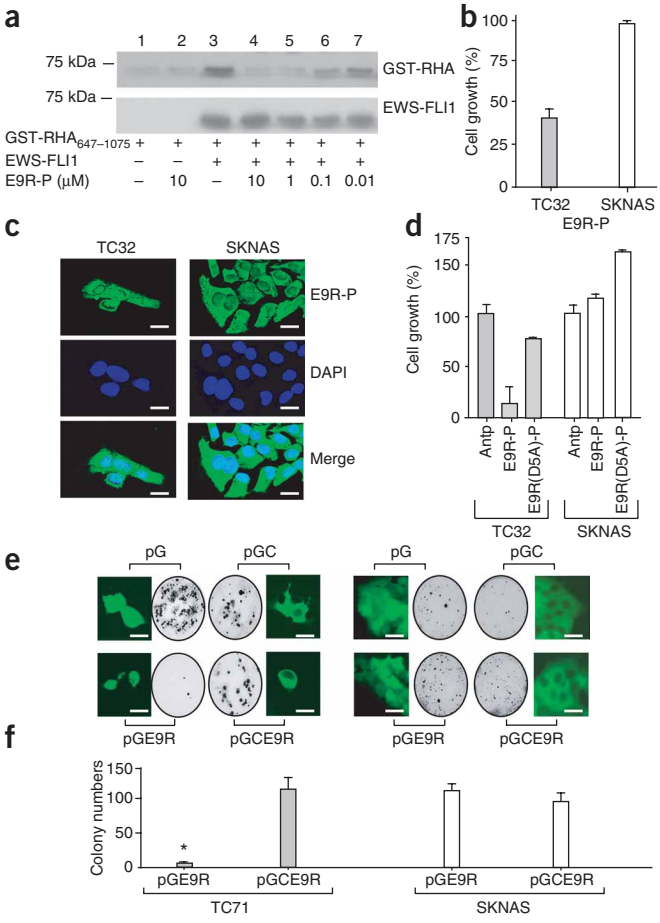

Figure 2 E9R peptide prevents EWS-FLI1 binding to RHA with specific detrimental effects upon ESFT growth and transformation. (**a**) Immunoprecipitation of GST-RHA$_{647–1075}$ using recombinant full-length EWS-FLI1 bound to a FLI1-specific antibody. (**b**) Growth reduction upon E9R-P (antennapedia-E9R) treatment (10 μM) in TC32 cells but not SKNAS cells. (**c**) E9R-P peptide uptake, tracked with FITC label (top images). DAPI nuclear counterstain (middle images) and merged (bottom images) are shown. Scale bar, 20 μm. (**d**) Graph showing growth response of TC32 and SKNAS cells to E9R–P, Antennapedia alone (Antp) or E9R-D5A-P. (**e**) TC71 and SKNAS cells expressing EGFP empty vector (pG), EGFP-E9R (pGE9R), EGFP with nuclear export sequence (pGC) or EGFP-E9R with nuclear export sequence (pGCE9R). (**f**) Average colony numbers of three experiments in TC71 cells expressing E9R throughout the cell. Scale bar, 20 μm.

E9R(D5A)-P, respectively; **Supplementary Table 1**). We treated monolayer cultures of the EWS-FLI1–positive ESFT cell line, TC32, or a control EWS-FLI1–negative cell line, SKNAS (neuroblastoma), with fluorescein-conjugated peptides. Only the EWS-FLI1–containing TC32 cells showed reduced growth with E9R peptide, and the SKNAS cells showed mild stimulation from the E9R peptide via an unknown mechanism (**Fig. 2b**). Confocal microscopy showed uptake throughout the cell, including nuclei (as evidenced by DAPI overlay, **Fig. 2c**). E9R-P significantly reduced ESFT cell growth ($P = 0.048$), while neither the D5A mutant control nor antennapedia peptides alone reduced ESFT cell growth (**Fig. 2d**). Neuroblastoma cells treated with the same peptides did not have a statistically significant alteration in growth, although we observed a slight increase with E9R(D5A)-P–treated cells ($P = 0.175$; **Fig. 2d**). To determine the effect of E9R on anchorage-independent growth, we cloned the E9R-encoding sequence into an EGFP-expressing plasmid (pGE9R). We also expressed EGFP-E9R peptide only in cytoplasm by adding a nuclear export signal sequence (LQLPPLERLTL) to the plasmid[28]. We stably transfected EGFP-E9R plasmid into TC71 (ESFT) or SKNAS (neuroblastoma) cells. Transfected cells showed E9R peptide expression either throughout the cell or excluded from the nucleus, as predicted on the basis of the intended targeting (**Fig. 2e**). TC71 colony formation was 95% lower owing to the expression of E9R, except when the peptide was excluded from the nucleus ($P = 0.0012$; **Fig. 2e,f**). The anchorage-independent growth of SKNAS was not affected by the E9R peptide (**Fig. 2e,f**). Further supporting the specificity of the E9R peptide, a second small round blue cell tumor, embryonal rhabdomyosarcoma, expressing pGE9R did not show reduced anchorage-independent growth (data not shown). Only expression of EGFP-E9R in TC71 reduced anchorage-independent growth (**Fig. 2e,f**).

Optimized small molecule binds to EWS-FLI1

We screened a library of 3,000 small molecules (National Cancer Institute Drug Targeting Program) for EWS-FLI1 binding by using surface plasmon resonance (SPR). We selected compounds that bind monomeric EWS-FLI1. We evaluated the binding state of the compound to EWS-FLI1 by the ratio of actual binding resonance units (RU_{actual}) to the theoretical binding resonance units (RU_{theor}). A ratio below 1.0 indicated monomeric binding of compound to EWS-FLI1. NSC635437 had an RU_{actual} to RU_{theor} ratio of 0.9, signifying monomeric binding to EWS-FLI1. NSC635437 had a greater potential to chemical derivatization with favorable drug-like properties[29]. We synthesized 1.0 g of NSC635437 to complete our studies and for use as a standard during compound optimization (**Fig. 3a**).

In a cell-free assay, NSC635437 reduced the direct binding of GST-RHA$_{647–1075}$ to full-length recombinant EWS-FLI1 (**Fig. 3b**). We used an aromatic optimization strategy to design analogs to improve the inhibition of RHA binding to EWS-FLI1 by NSC635437. One of these compounds (YK-4-279), substituted with a methoxy group at the para position (*p*-methoxy) of the aromatic ring (**Fig. 3a**), markedly reduced the protein-protein interaction of EWS-FLI1 with GST-RHA$_{647–1075}$ *in vitro* (**Fig. 3b**). We calculated a K_D of 9.48 μM for the affinity of YK-4-279 with EWS-FLI1 by SPR (**Fig. 3c**). To support a model of YK-4-279 as having similar interaction qualities to E9R, we used an SPR displacement assay to show that 10 μM YK-4-279 reduces the binding of 64 μM E9R from 17 RU to 7 RU, and 32 μM E9R reduces the binding from 13 RU to 5 RU (**Fig. 3d**). YK-4-279 at 30 μM completely displaced E9R from EWS-FLI1 binding, as measured by fluorescence polarization assay (**Fig. 3e**).

YK-4-279 functionally inhibits EWS-FLI1 and ESFT cells

ESFT cells treated with YK-4-279 showed a dissociation of EWS-FLI1 from RHA by 10 μM, consistent with the K_D value (**Fig. 4a**). YK-4-279 did not directly affect EWS-FLI1 or RHA levels (**Fig. 4a** and **Supplementary Fig. 3**). To further support YK-4-279 as a functional inhibitor of EWS-FLI1, we transfected COS7 cells with EWS-FLI1 and NR0B1 reporter-luciferase plasmid (containing EWS-FLI1 regulatory GGAA elements[30]). The EWS-FLI1–transfected cells showed a dose-dependent decrease in promoter activity when treated for 18 h with 3 μM and 10 μM YK-4-279 (**Fig. 4b,c**). As an additional control for nonspecific promoter effects, we transfected an NF-κB–responsive reporter into COS7 cells and activated it with phorbol 12-myristate 13-acetate. YK-4-279 did not affect the NF-κB–responsive promoter (**Supplementary Fig. 4a**). In a recent publication, EWS-FLI1 was

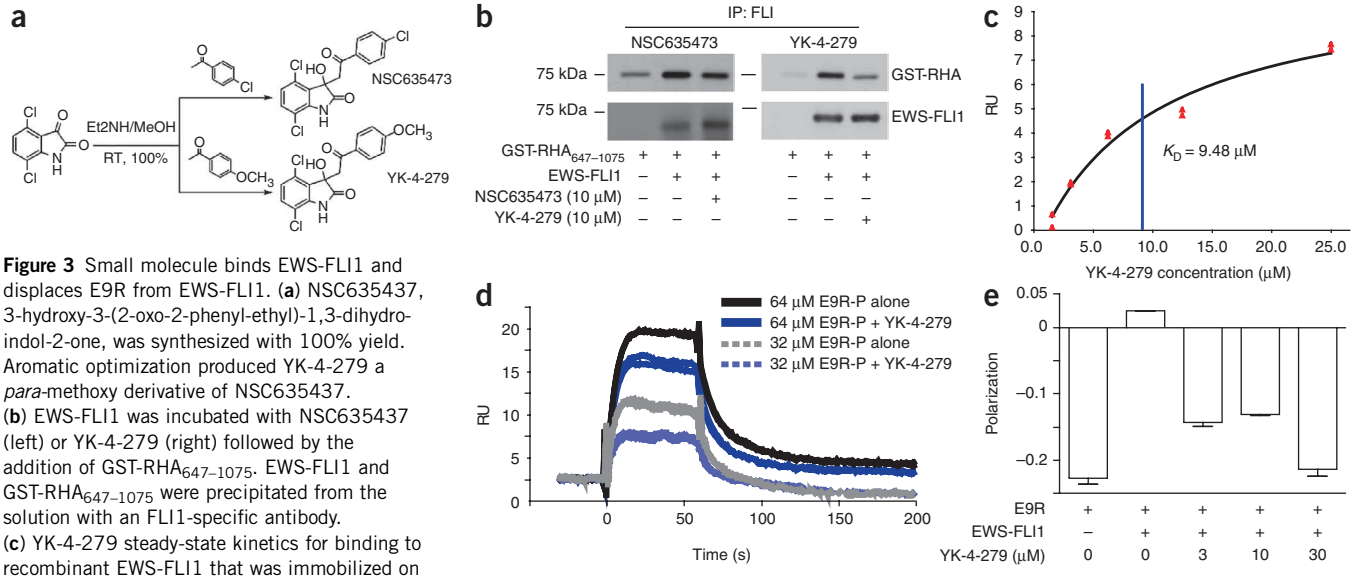

Figure 3 Small molecule binds EWS-FLI1 and displaces E9R from EWS-FLI1. (**a**) NSC635437, 3-hydroxy-3-(2-oxo-2-phenyl-ethyl)-1,3-dihydro-indol-2-one, was synthesized with 100% yield. Aromatic optimization produced YK-4-279 a *para*-methoxy derivative of NSC635437. (**b**) EWS-FLI1 was incubated with NSC635437 (left) or YK-4-279 (right) followed by the addition of GST-RHA$_{647–1075}$. EWS-FLI1 and GST-RHA$_{647–1075}$ were precipitated from the solution with an FLI1-specific antibody. (**c**) YK-4-279 steady-state kinetics for binding to recombinant EWS-FLI1 that was immobilized on a CM5 Biacore chip. (**d**) SPR displacement assay of 64 μM E9R alone and with addition of YK-4-279; 32 μM E9R alone and with addition of YK-4-279. (**e**) Graph showing YK-4-279 displacement of E9R-P from EWS-FLI1, as measured by fluorescent polarization.

shown to modulate cyclin D1 protein abundance by altering a cyclin D1 splice site[31]. Blocking the interaction of EWS-FLI1 with RHA using YK-4-279 nearly eliminated cyclin D1 in TC32 cells treated for 14 h (**Fig. 4d**) but did not affect cyclin D1 expression in four non–EWS-FLI1–containing cell lines (**Supplementary Fig. 4b,c**).

We found that NSC635437 has a half-maximal inhibitory concentration (IC_{50}) of 20 μM for TC32 cells growing in monolayer; however, the derivative, YK-4-279, reduced the IC_{50} to 900 nM (**Fig. 5a**). YK-4-279 was relatively specific for ESFT cells as compared to the nontransformed HEK293 cells, showing a tenfold difference in IC_{50} (**Fig. 5b**). Primary cell lines, ES925 and GUES1, established from individuals with ESFTs with recurrent tumors showed sensitivity to YK-4-279 with antiproliferative IC_{50} values of 1 μM and 8 μM, respectively (**Fig. 5c**). A panel of ESFT cell lines showed IC_{50} values between 0.5 μM and 2 μM for YK-4-279, whereas cell lines that lack EWS-FLI1 had IC_{50} values in excess of 25 μM (**Fig. 5d**). An additional panel of nontransformed human foreskin keratinocytes (HFK cells) and human ectocervical cells (HEC cells) treated for 3 d with 30 μM YK-4-279 showed an IC_{50} that exceeded 30 μM (**Supplementary Fig. 5a**).

As an apoptotic indicator, caspase-3 activity[32] rose in a dose-dependent fashion in TC32 cells treated with YK-4-279 for 24 h (**Supplementary Fig. 5b**). Caspase-3 activation in response to YK-4-279 was similar to that induced by doxorubicin, a standard agent in the treatment of patients with ESFT[6]. We evaluated additional malignant and nonmalignant cell lines for caspase-3 activation in response to YK-4-279. YK-4-279 induced caspase-3 activity in four ESFT cell lines (TC32, A4573, TC71 and ES925 cells), however none of the five non–EWS-FLI1 cancer cell lines nor any of the three nontransformed cell lines (HFK, HEC and HEK293 cells) treated with YK-4-279 underwent apoptosis (**Fig. 5e**). Treatment of TC32, HEK293, HFK and HEC cells with short-term (6-h) high-dose (50 μM) YK-4-279 resulted in substantial apoptosis of the ESFT cells but no death of the nontransformed cells (**Fig. 5f**). Together, these results support the specific toxicity of YK-4-279 in tumor cell lines containing EWS-FLI1 compared with other tumor and non-transformed cells.

To further support for the target specificity of YK-4-279 toxicity in ESFT cells, we reduced the levels of EWS-FLI1 and RHA proteins by using shRNA in A673 cells[33]. Cells with knocked down RHAR showed a YK-4-279 IC_{50} of >10 μM, whereas cells treated with the control shRNA (targeting luciferase) had a YK-4-279 IC_{50} of less than 1 μM (**Supplementary Fig. 5c**). When we lowered EWS-FLI1 expression with shRNA, the IC_{50} increased tenfold from 0.5 μM to approximately 5 μM (**Supplementary Fig. 5d,e**).

ESFT xenograft growth is inhibited by YK-4-279

We established ESFT (orthotopic) with CHP-100 and TC71 or prostate cancer with PC3 cell xenograft tumors in severe combined

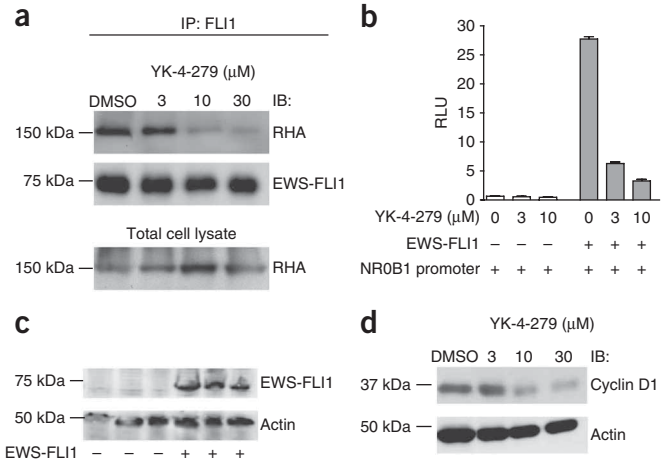

Figure 4 YK-4-279 reduces EWS-FLI1 functional activity. (**a**) TC32 cells were treated with YK-4-279, and resolved protein lysates were immunoblotted for co-precipitated RHA (top), EWS-FLI1 (middle) or total RHA (bottom). IP, immunoprecipitate; IB, immunoblot. (**b**) Luciferase reporter assay of the EWS-FLI1–responsive NR0B1 promoter upon dose-dependent (18-h) YK-4-279 treatment in COS7 cells. (**c**) Protein lysates from transfected cells showing expression of EWS-FLI1. (**d**) YK-4-279–treated TC32 cell lysates (treated for 14 h) were blotted for cyclin D1 and actin.

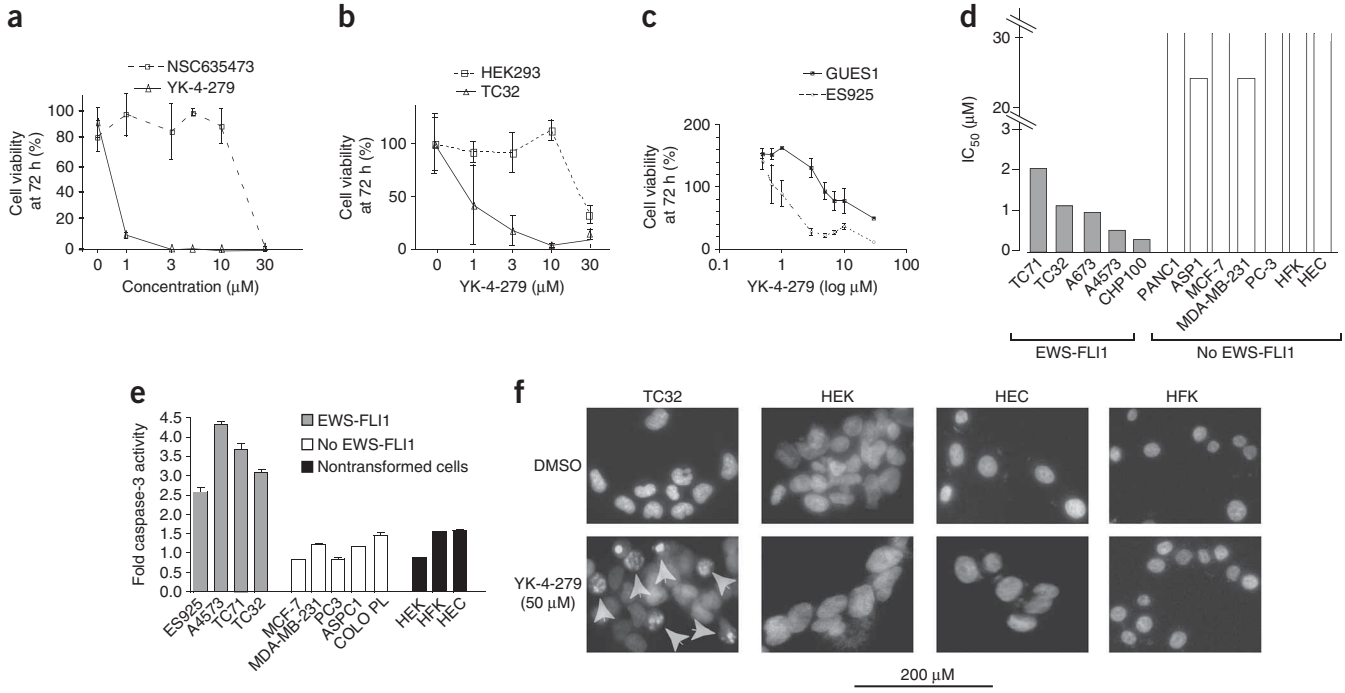

Figure 5 YK-4-279 is a potent and specific inhibitor of ESFTs. (**a**) TC32 cells were treated with a dose range of YK-4-279 and NSC635437. Cell growth, as measured by 3-(4, 5-Dimethyl-2-thiazolyl)-2, 5-diphenyl-2H-tetrazolium bromide (MTT) or WST reduction after 7 d in culture. (**b**) TC32 and HEK293 (nontransformed, lacking EWS-FLI1) cells were treated similarly to those in **a**. (**c**) Primary ESFT explant cell lines GUES1 and ES925 were treated for 3 d with YK-4-279. (**d**) Cell lines expressing EWS-FLI1 were compared to non–EWS-FLI1 malignant cell lines after 3 d in culture to establish the IC_{50} using WST assay. (**e**) Caspase-3 activity of a panel of ESFT (TC32, TC71, A4573 and ES925), malignant non–EWS-FLI1–expressing (MCF-7, MDA-MB-231, PC3, ASPC1 and COLO-PL) and nontransformed (HEK-293, HFK and HEC) cells. Graph shows fluorescence in treated lysate divided by that of untreated lysate. (**f**) Arrows indicate apoptotic nuclear fragmentation after 50 μM YK-4-279 treatment of ESFT (TC32) cells and nontransformed cells (HEK-293, HFK and HEC). Scale bar, 200 μm.

immunodeficient–beige mice. The tumor growth rate of YK-4-279–treated mice bearing CHP-100 (**Fig. 6a**) was lower than that in mice having PC3 prostate tumors (**Fig. 6b**). The cumulative data from five independent experiments with the ESFT xenografts (TC71 and CHP-100) show a marked overall tumor reduction ($P < 0.0001$) in the YK-4-279–treated mice (**Fig. 6c**). Pathological analysis of mice treated with YK-4-279 did not show any signs of toxicity, except for sterile inflammatory lesions in the abdominal cavities of mice, where

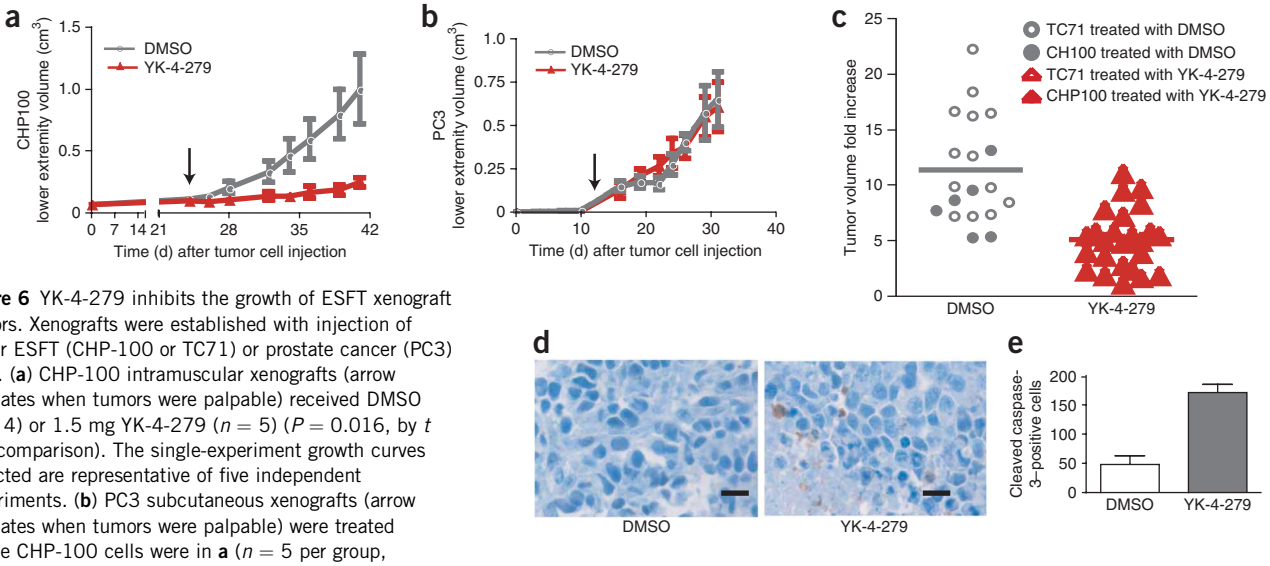

Figure 6 YK-4-279 inhibits the growth of ESFT xenograft tumors. Xenografts were established with injection of either ESFT (CHP-100 or TC71) or prostate cancer (PC3) cells. (**a**) CHP-100 intramuscular xenografts (arrow indicates when tumors were palpable) received DMSO ($n = 4$) or 1.5 mg YK-4-279 ($n = 5$) ($P = 0.016$, by t test comparison). The single-experiment growth curves depicted are representative of five independent experiments. (**b**) PC3 subcutaneous xenografts (arrow indicates when tumors were palpable) were treated as the CHP-100 cells were in **a** ($n = 5$ per group, representative of three independent experiments). (**c**) Overall response of ESFT xenografts (TC71 and CHP-100) to YK-4-279 (1.5 mg per dose). Tumor volumes at day 14 after treatment initiation compared across five experiments are shown (DMSO, $n = 19$; YK-4-279, $n = 25$; $P < 0.0001$, by Mann-Whitney test). (**d**) Tumors from the mice in **a** were analyzed by immunohistochemistry for activation of caspase-3 activity. (**e**) Caspase-3–positive cells were counted ($n > 500$ in three high-power fields) in four separately stained slides for each group ($P = 0.041$).

intraperitoneal injections were applied. Tumors from mice treated with YK-4-279 were compared with those after DMSO treatment by immunohistochemistry to identify caspase-3 activity (**Fig. 6d**). The CHP-100 xenograft tumors from treated mice had a threefold increase in caspase-3 activity compared to control mice (**Fig. 6e**). These results show inhibition of tumor growth and concomitant increased apoptosis after YK-4-279 treatment in two models of ESFT.

DISCUSSION

EWS-FLI1 is a unique, cancer-specific molecule that is a potential therapeutic target in ESFT cells. RHA is essential for the function of EWS-FLI1. We showed that an E9R peptide that blocks RHA binding to EWS-FLI1 (E9R) specifically reduced the transformation activity of EWS-FLI1. We also identified a small-molecule lead compound that binds EWS-FLI1. The lead compound derivative, YK-4-279, along with E9R peptide, shows that the EWS-FLI1–RHA interaction can be blocked with a detrimental effect on ESFT cells both *in vitro* and *in vivo*. These findings validate a highly specific cancer target, the interaction of EWS-FLI1 with RHA.

These are to our knowledge the first experiments that evaluate a small-molecule inhibitor of EWS-FLI1 function. A series of xenograft experiments show that 60–75 mg per kg body weight YK-4-279 substantially decreases tumor growth. The small molecule not only inhibits RHA binding to EWS-FLI1 but also decreases EWS-FLI1 modulated transcription, on the basis of reporter assays. An additional putative function of EWS-FLI1 is splice-site modification[34], which was recently supported by the EWS-FLI1–altered splicing of cyclin D1 (ref. 31). Treatment of ESFT cells with YK-4-279 led to decreased cyclin D1 levels. Additional investigations of the splicing complex are necessary to determine whether this effect is due to the disruption of an EWS-FLI1–RHA complex or allosteric interference with EWS-FLI1. Small-molecule inhibitors of protein-protein interactions have great therapeutic potential and will be immediately useful as functional probes.

EWS-FLI1 was recognized as a potential therapeutic target over 15 years ago, almost immediately after the protein was identified as a product of the breakpoint region t(11;22)[35]. We hypothesized that RHA is a functionally crucial partner of EWS-FLI1. We developed small-molecule protein-protein interaction inhibitors against EWS-FLI1 and RHA without benefit of a fixed structure of EWS-FLI1. The exact nature of the requirement of RHA by EWS-FLI1 is currently under investigation; however, we speculate that RHA could be involved in EWS-FLI1 function, synthesis or stability. Our data support multiple mechanisms and therefore require further enzymatic and structural studies of EWS-FLI1–bound RHA for resolution. The fact that YK-4-279 is still toxic to A673 cells with low EWS-FLI1 expression could be due to residual EWS-FLI1 or suggest broader action of the compound. In addition, although our data suggest that YK-4-279 has ESFT cell-specific toxic effects, we recognize that as additional cell and tumor models are tested, other protein interactions of YK-4-279 may be revealed.

Inhibitory peptides offer a higher likelihood of specificity than small molecules to validate protein-protein interaction targets and to evaluate protein-complex disruption; however, peptides are problematic for clinical development. Although small peptides are currently being developed as therapeutic agents[36,37], 10–20–amino acid peptides present formidable pharmacokinetic stability and delivery challenges. Our investigations use peptides to compare the effects of disrupting protein-protein interactions with our small molecules. The E9R peptide may compete with full-length RHA binding to EWS-FLI1, and our data support a functional displacement of RHA by E9R. Small molecule YK-4-279 can 'displace' E9R peptide from EWS-FLI1, as shown by SPR and fluorescence polarization. Although our results support E9R and YK-4-279 binding to the same site on EWS-FLI1, allosteric interference cannot be excluded. Therefore, a structural model of EWS-FLI1 is required to fully prove both this interaction and the YK-4-279 binding site but is yet unavailable owing to the challenges of disordered proteins[23].

The interaction of RHA with EWS-FLI1 presents an ideal opportunity for the development of small-molecule protein-protein interaction inhibitors. Both the evidence and the prevailing opinion support disordered proteins as potential targets of small molecule therapeutics[38]. Our data also support EWS-FLI1 protein interaction targeting to modulate oncogene function and potentially lead to new therapeutics. Additional experiments to evaluate multispecies specificity, toxicity and absorption, distribution, metabolism and excretion are required to advance a further optimized derivative of YK-4-279 into clinical trials. Small molecules that disable EWS-FLI1 function with minimal toxicity, in particular sparing hematopoetic stem cells, could potentially provide a valuable adjuvant therapy for patients with ESFT. In addition, this paradigm for drug discovery could be applied to many related sarcomas that share similar oncogenic fusion proteins.

METHODS

Methods and any associated references are available in the online version of the paper at http://www.nature.com/naturemedicine/.

Note: Supplementary information is available on the Nature Medicine website.

ACKNOWLEDGMENTS

This work was generously supported by the Children's Cancer Foundation of Baltimore (J.T. and A.Ü.), Go4theGoal Foundation (J.T.), Dani's Foundation of Denver (J.T.), the Liddy Shriver Sarcoma Initiative (J.T.), the Amschwand Sarcoma Cancer Foundation (J.T.), the Burroughs-Wellcome Clinical Scientist Award in Translational Research (J.T.), US National Institutes of Health grants R01CA138212 (J.T.) and R01CA133662 (J.T.), and the Georgetown University Medical Center Drug Discovery Program. US National Institutes of Health support is through the Cancer Center Support Grant P30 CA051008 for use of Flow Cytometry and Cell Sorting, Biacore Molecular Interaction, Tissue Culture and microscopy core facilities and grant P01 CA47179 (M.M.). We would like to thank S. Metallo for training in fluorescence polarization. Also, T. Cripe and L. Whitesell provided critical review of our manuscript. We also thank S. Lessnick from Hunstamn Cancer Institute, for providing NROB1 reporter plasmid, J.V. Frangioni from Beth Israel Deaconess Medical Center for providing pG, pGN and pGC vectors, O. Delattre from INSERM France for providing the A673 shEWS-FLI1 cell line, and R. Schlegel, Lombardi Comprehensive Cancer Center, for providing HFK and HEC cell lines. We thank the Developmental Therapeutics Program of the US National Cancer Institute for providing the Diversity set of compounds for screening. This article is dedicated to our patients who have fought but succumbed to ESFT.

AUTHOR CONTRIBUTIONS

H.V.E., J.S.B.-R., M.M., L.Y., O.D.A., S.S., T.-h.C., A.Ü. and J.A.T. designed and carried out experiments. Y.K., S.D. and M.L.B. designed and synthesized chemical compounds. H.V.E. and J.A.T. wrote the manuscript. All authors reviewed, critiqued and offered comments to the text.

COMPETING INTERESTS STATEMENT

The authors declare competing financial interests: details accompany the full-text HTML version of the paper at http://www.nature.com/naturemedicine/.

Published online at http://www.nature.com/naturemedicine/
Reprints and permissions information is available online at http://npg.nature.com/reprintsandpermissions/

1. Mitelman, F., Johansson, B. & Mertens, F. The impact of translocations and gene fusions on cancer causation. *Nat. Rev. Cancer* **7**, 233–245 (2007).
2. French, C.A. *et al.* Midline carcinoma of children and young adults with NUT rearrangement. *J. Clin. Oncol.* **22**, 4135–4139 (2004).
3. Helman, L.J. & Meltzer, P. Mechanisms of sarcoma development. *Nat. Rev. Cancer* **3**, 685–694 (2003).

4. Poppe, B. *et al.* Expression analyses identify MLL as a prominent target of 11q23 amplification and support an etiologic role for MLL gain of function in myeloid malignancies. *Blood* **103**, 229–235 (2004).
5. Carroll, M. *et al.* CGP 57148, a tyrosine kinase inhibitor, inhibits the growth of cells expressing BCR-ABL, TEL-ABL, and TEL-PDGFR fusion proteins. *Blood* **90**, 4947–4952 (1997).
6. Grier, H.E. *et al.* Addition of ifosfamide and etoposide to standard chemotherapy for Ewing's sarcoma and primitive neuroectodermal tumor of bone. *N. Engl. J. Med.* **348**, 694–701 (2003).
7. Delattre, O. *et al.* The Ewing family of tumors—a subgroup of small-round-cell tumors defined by specific chimeric transcripts. *N. Engl. J. Med.* **331**, 294–299 (1994).
8. Hu-Lieskovan, S., Heidel, J.D., Bartlett, D.W., Davis, M.E. & Triche, T.J. Sequence-specific knockdown of EWS-FLI1 by targeted, nonviral delivery of small interfering RNA inhibits tumor growth in a murine model of metastatic Ewing's sarcoma. *Cancer Res.* **65**, 8984–8992 (2005).
9. Kovar, H., Ban, J. & Pospisilova, S. Potentials for RNAi in sarcoma research and therapy: Ewing's sarcoma as a model. *Semin. Cancer Biol.* **13**, 275–281 (2003).
10. Tanaka, K., Iwakuma, T., Harimaya, K., Sato, H. & Iwamoto, Y. EWS-Fli1 antisense oligodeoxynucleotide inhibits proliferation of human Ewing's sarcoma and primitive neuroectodermal tumor cells. *J. Clin. Invest.* **99**, 239–247 (1997).
11. Petermann, R. *et al.* Oncogenic EWS-Fli1 interacts with hsRPB7, a subunit of human RNA polymerase II. *Oncogene* **17**, 603–610 (1998).
12. Nakatani, F. *et al.* Identification of p21WAF1/CIP1 as a direct target of EWS-Fli1 oncogenic fusion protein. *J. Biol. Chem.* **278**, 15105–15115 (2003).
13. Toretsky, J.A. *et al.* Oncoprotein EWS-FLI1 activity is enhanced by RNA helicase A. *Cancer Res.* **66**, 5574–5581 (2006).
14. Lee, C.G. *et al.* RNA helicase A is essential for normal gastrulation. *Proc. Natl. Acad. Sci. USA* **95**, 13709–13713 (1998).
15. Hartman, T.R. *et al.* RNA helicase A is necessary for translation of selected messenger RNAs. *Nat. Struct. Mol. Biol.* **13**, 509–516 (2006).
16. Tetsuka, T. *et al.* RNA helicase A interacts with nuclear factor κB p65 and functions as a transcriptional coactivator. *Eur. J. Biochem.* **271**, 3741–3751 (2004).
17. Välineva, T., Yang, J. & Silvennoinen, O. Characterization of RNA helicase A as component of STAT6-dependent enhanceosome. *Nucleic Acids Res.* **34**, 3938–3946 (2006).
18. Myöhänen, S. & Baylin, S.B. Sequence-specific DNA binding activity of RNA helicase A to the p16INK4a promoter. *J. Biol. Chem.* **276**, 1634–1642 (2001).
19. Zhong, X. & Safa, A.R. RNA helicase A in the MEF1 transcription factor complex up-regulates the *MDR1* gene in multidrug-resistant cancer cells. *J. Biol. Chem.* **279**, 17134–17141 (2004).
20. Nakajima, T. *et al.* RNA helicase A mediates association of CBP with RNA polymerase II. *Cell* **90**, 1107–1112 (1997).
21. Anderson, S.F., Schlegel, B.P., Nakajima, T., Wolpin, E.S. & Parvin, J.D. BRCA1 protein is linked to the RNA polymerase II holoenzyme complex via RNA helicase A. *Nat. Genet.* **19**, 254–256 (1998).
22. Robb, G.B. & Rana, T.M. RNA helicase A interacts with RISC in human cells and functions in RISC loading. *Mol. Cell* **26**, 523–537 (2007).
23. Bhalla, J., Storchan, G.B., MacCarthy, C.M., Uversky, V.N. & Tcherkasskaya, O. Local flexibility in molecular function paradigm. *Mol. Cell. Proteomics* **5**, 1212–1223 (2006).
24. Xie, H. *et al.* Functional anthology of intrinsic disorder. 1. Biological processes and functions of proteins with long disordered regions. *J. Proteome Res.* **6**, 1882–1898 (2007).
25. Ng, K.P. *et al.* Multiple aromatic side chains within a disordered structure are critical for transcription and transforming activity of EWS family oncoproteins. *Proc. Natl. Acad. Sci. USA* **104**, 479–484 (2007).
26. Üren, A., Tcherkasskaya, O. & Toretsky, J.A. Recombinant EWS-FLI1 oncoprotein activates transcription. *Biochemistry* **43**, 13579–13589 (2004).
27. Terrone, D., Sang, S.L., Roudaia, L. & Silvius, J.R. Penetratin and related cell-penetrating cationic peptides can translocate across lipid bilayers in the presence of a transbilayer potential. *Biochemistry* **42**, 13787–13799 (2003).
28. Voss, S.D., DeGrand, A.M., Romeo, G.R., Cantley, L.C. & Frangioni, J.V. An integrated vector system for cellular studies of phage display-derived peptides. *Anal. Biochem.* **308**, 364–372 (2002).
29. Leeson, P.D. & Springthorpe, B. The influence of drug-like concepts on decision-making in medicinal chemistry. *Nat. Rev. Drug Discov.* **6**, 881–890 (2007).
30. Gangwal, K. *et al.* Microsatellites as EWS/FLI response elements in Ewing's sarcoma. *Proc. Natl. Acad. Sci. USA* **105**, 10149–10154 (2008).
31. Sanchez, G. *et al.* Alteration of cyclin D1 transcript elongation by a mutated transcription factor up-regulates the oncogenic D1b splice isoform in cancer. *Proc. Natl. Acad. Sci. USA* **105**, 6004–6009 (2008).
32. Li, F. *et al.* Control of apoptosis and mitotic spindle checkpoint by survivin. *Nature* **396**, 580–584 (1998).
33. Knoop, L.L. & Baker, S.J. EWS/FLI alters 5′-splice site selection. *J. Biol. Chem.* **276**, 22317–22322 (2001).
34. Tirode, F. *et al.* Mesenchymal stem cell features of Ewing tumors. *Cancer Cell* **11**, 421–429 (2007).
35. Delattre, O. *et al.* Gene fusion with an ETS DNA-binding domain caused by chromosome translocation in human tumours. *Nature* **359**, 162–165 (1992).
36. Plescia, J. *et al.* Rational design of shepherdin, a novel anticancer agent. *Cancer Cell* **7**, 457–468 (2005).
37. Palermo, C.M., Bennett, C.A., Winters, A.C. & Hemenway, C.S. The AF4-mimetic peptide, PFWT, induces necrotic cell death in MV4–11 leukemia cells. *Leuk. Res.* **32**, 633–642 (2008).
38. Cheng, Y. *et al.* Rational drug design via intrinsically disordered protein. *Trends Biotechnol.* **24**, 435–442 (2006).

ONLINE METHODS

Materials. We obtained E9R peptide from Bio-synthesis. We obtained protein G beads (Invitrogen), antibody to GST, antibody to FLI1, antibody to cyclin D1 (all from Santa Cruz), fluorogenic caspase-3 substrate *N*-acetyl-Asp-Glu-Val-Asp-**AMC** (7-amino-4- methylcoumarin) (Ac-DEVD-AMC), caspase-3 fluorogenic substrate (BD Biosciences Pharmingen) and antibody to cleaved caspase 3 (Asp175) (Cell Signaling) from commercial sources.

Site-directed mutagenesis. We changed every nonalanine amino acid in the amino acids 823–832 region of RHA to alanine by site-directed mutagenesis with QuickChange II XL Site-Directed Mutagenesis Kit (Stratagene) according to the manufacturer's protocol.

Cell cultures. We maintained established TC32, TC71, A4573, CHP-100 and primary ES925 and GUES1 ESFT cell lines in RPMI (Invitrogen) medium supplemented with 10% FBS (Gemini Bioproducts). HEC and HFK cell lines, kind gifts from R. Schlegel, are previously described[39]. We tested subclones of these cells stably expressing EWS-FLI1 tested in an anchorage-independent growth assay as previously described[13].

Protein immunoprecipitation assays. We made protein lysates and performed immunoprecipitations as previously published[13]. We prepared recombinant GST-RHA$_{647–1075}$ from crude bacterial extracts without further purification.

Small molecule library screening and selection of lead compound. We established an SPR assay using the Biacore T100 with EWS-FLI1, prepared in our laboratory as previously published[26]. We used DNA oligonucleotides to quality-control the proper conformation of EWS-FLI1 on the surface of a CM5 chip. We prioritized small molecules from the Developmental Therapeutics Program of the National Cancer Institute, US National Institutes of Health on the basis of their molecular weight and solubility. We performed an initial screening of molecules at 1 μM or 10 μM compound, based on solubility. We used a model that compares the actual binding maximum (actual RU) with the theoretical binding maximum (RU$_{theor}$). If the RU$_{actual}$ to RU$_{theor}$ ratio is 0.9–1.0, this suggests a binding, and such a compound is considered a 'hit'. A team of medicinal chemists then reviewed hits, and those with structural potentials were selected for further study. We tested selected molecules *in vitro* in a solution co-immunoprecipitation assay with recombinant EWS-FLI1 and GST-RHA$_{647–1075}$.

Synthesis and analysis of small molecule compounds. Details provided in the **Supplementary Methods**.

Fluorescence polarization assay. We added increasing concentrations of FITC-E9R to a fixed concentration of EWS-FLI1 (4.8 μM) to obtain a saturated binding curve. We performed the assay in 20 mM Tris, 500 mM NaCl and 0.67M imidazole, pH 7.4. We analyzed the fluorescence polarization in a QuantaMaster fluorimeter (Photon Technology International) equipped with polymer sheet polarizers at an excitation wavelength of 495 nm and emission wavelength of 517 nm. We added increasing concentrations of YK-4-279 to a fixed concentration of EWS-FLI1 and FITC-E9R (3.2 μM, as determined from saturated binding curve) with the same buffer and instrumental settings as described above.

Plasmids and reporter assay. We prepared EGFP-E9R fusion constructs as previously published[40]. We transiently transfected the NR0B1 (ref. 31) luciferase reporter and full-length EWS-FLI1 into COS-7 cells with Fugene-6 (Roche) and performed the luciferase assay per the manufacturer's protocol (Dual Luciferase Kit, Promega). Six hours after transfection, we treated cells with either 3 μM or 10 μM YK-4-279. We standardized cell lysate luciferase activity to *Renilla* activity from a nonaffected promoter and plotted as relative luciferase activity (RLA).

Caspase-3 activity measurement and nuclear fragmentation. We treated cells for 24 h with 10 μM YK-4-279. We incubated the Caspase-3 substrate DEVD-AMC with equal amounts of protein lysate and measured the fluorescence from cleaved substrate in a fluorimeter. We treated TC32 cells and nontransformed HEK-293, HFK and HEC cells for 6 h with high-dose (50 μM) YK-4-279. We photographed DAPI-stained cells at 600× magnification on an inverted fluorescence microscope.

Mouse strains and *in vivo* small-molecule testing. We orthotopically injected 1 million TC71 or CHP-100 cells in 100 μl HBSS into the gastrocnemius muscle of 4- to 8-week-old severe combined immunodeficient–beige mice (Taconic). We established prostate cancer xenografts by subcutaneous injection of 5 million PC3 cells into the flanks of 4- to 8-week-old nude mice (Taconic). We randomized mice to treatment groups receiving thrice weekly intraperitoneal injections of DMSO or YK-4-279 at 1.5 mg per dose when tumors were palpable. We began each of the mouse experiments with ten mice that were randomized into treatment and control groups when the tumors reached palpable size. In the control groups, some tumors exceeded the Institutional Animal Care and Use Committee maximal size (2 cm in any dimension) and were euthanized before day 14 and thus not included in the day 14 analysis (**Fig. 6c**). We measured tumor length and width every 2–4 d and calculated volume with the formula volume $= D \times d^2 \times \pi/6$, where D is the longest diameter and d is the shorter diameter. Xenograft studies were approved by the Memorial Sloan-Kettering Cancer Center Institutional Animal Care and Use Committee.

Statistical analyses. We performed statistical analyses with GraphPad Prism.

39. Uren, A. *et al.* Activation of the canonical Wnt pathway during genital keratinocyte transformation: a model for cervical cancer progression. *Cancer Res.* **65**, 6199–6206 (2005).
40. Frangioni, J.V. & Neel, B.G. Use of a general purpose mammalian expression vector for studying intracellular protein targeting: identification of critical residues in the nuclear lamin A/C nuclear localization signal. *J. Cell Sci.* **105**, 481–488 (1993).

doi:10.1038/nm.1983

Supplementary Figure Legends:

Supplementary Figure 1. Pancreatic cells survive when RHA levels are decreased. PANC1 cells were infected with virus containing either siRNA for RHA or control luciferase. a. Immunoblot showing protein levels following 6 days of selection. b. Viability of cells using WST reduction 6 days after selection and RHA reduction.

Supplementary Figure 2. RHA ATPase activity lost with P824A mutation but not D827A. a. ATPase assay was performed as previously published, except the Biomol Green was used to detect free phosphate. While the P824A mutant did show reduced ATPase activity, the D827A mutation did not affect RHA function. Phosphate standards were used to calibrate the assay and determine the rate of ATP hydrolysis. RHA(K417R) is a known NTPase-null mutant of RHA. Immunoglobulin control immunoprecipitations did not demonstrate ATPase activity (data not shown). b. Protein levels shown by immunoblot.

Supplementary Figure 3. RHA levels are not reduced by YK-4-279treatment. Immunoblot from log-phase cell lysates that were either treated with DMSO control or 10 μM YK-4-279 overnight.

Supplementary Figure 4. YK-4-279 does not reduce NF-kB activity nor cyclin D levels in non-ESFT cells. a. COS7 cells were transfected with an NFκB reporter construct followed by stimulation with PMA. Cells were treated with YK-4-279 following PMA treatment. Cell lysates were analyzed for NFκB induced luciferase activity as standardized to LTR activated renilla luciferase. b. Immunoblot from log-phase cell lysates that were either treated with DMSO control or 10 μM YK-4-279 overnight. c. Graph shows densitometry of treated/untreated with both standardized for β-tubulin expression.

Supplementary Figure 5. Additional studies evaluating specificity of YK-4-279. a. HEC and HFK, non-transformed endocervical cells and keritinocytes, were treated YK-4-279 for 72 hours and assayed for viability using WST reduction. b. TC71 cells were treated for 16 hours with YK-4-279 or doxorubicin. Lysates were assayed for cleavage of AMC-DEVD by induced caspase-3 and fluorescence was measured. c. RHA reduced TC71 cells were more resistant to YK-4-279 treatment than wild-type cells. d. An shRNA tet-inducible expression vector was stably transfected into A673 (ESFT) cells to reduce EWS-FLI1 levels. e. EWS-FLI1 reduced A673 cells were more resistant to YK-4-279 treatment than wild-type cells.

Supplementary Figure Legends:

Supplementary Figure 1. Pancreatic cells survive when RHA levels are decreased. PANC1 cells were infected with virus containing either siRNA for RHA or control luciferase. a. Immunoblot showing protein levels following 6 days of selection. b. Viability of cells using WST reduction 6 days after selection and RHA reduction.

Supplementary Figure 2. RHA ATPase activity lost with P824A mutation but not D827A. a. ATPase assay was performed as previously published, except the Biomol Green was used to detect free phosphate. While the P824A mutant did show reduced ATPase activity, the D827A mutation did not affect RHA function. Phosphate standards were used to calibrate the assay and determine the rate of ATP hydrolysis. RHA(K417R) is a known NTPase-null mutant of RHA. Immunoglobulin control immunoprecipitations did not demonstrate ATPase activity (data not shown). b. Protein levels shown by immunoblot.

Supplementary Figure 3. RHA levels are not reduced by YK-4-279treatment. Immunoblot from log-phase cell lysates that were either treated with DMSO control or 10 μM YK-4-279 overnight.

Supplementary Figure 4. YK-4-279 does not reduce NF-kB activity nor cyclin D levels in non-ESFT cells. a. COS7 cells were transfected with an NFκB reporter construct followed by stimulation with PMA. Cells were treated with YK-4-279 following PMA treatment. Cell lysates were analyzed for NFκB induced luciferase activity as standardized to LTR activated renilla luciferase. b. Immunoblot from log-phase cell lysates that were either treated with DMSO control or 10 μM YK-4-279 overnight. c. Graph shows densitometry of treated/untreated with both standardized for β-tubulin expression.

Supplementary Figure 5. Additional studies evaluating specificity of YK-4-279. a. HEC and HFK, non-transformed endocervical cells and keritinocytes, were treated YK-4-279 for 72 hours and assayed for viability using WST reduction. b. TC71 cells were treated for 16 hours with YK-4-279 or doxorubicin. Lysates were assayed for cleavage of AMC-DEVD by induced caspase-3 and fluorescence was measured. c. RHA reduced TC71 cells were more resistant to YK-4-279 treatment than wild-type cells. d. An shRNA tet-inducible expression vector was stably transfected into A673 (ESFT) cells to reduce EWS-FLI1 levels. e. EWS-FLI1 reduced A673 cells were more resistant to YK-4-279 treatment than wild-type cells.

Supplementary Figure 4